

Ocean Surface Wave Optical Roughness – Analysis of Innovative Measurements

Christopher J. Zappa
Lamont-Doherty Earth Observatory of Columbia University
Ocean and Climate Physics Division
61 Route 9W
Palisades, NY 10964
Phone: (845) 365-8547 fax: (845) 365-8157 email: zappa@ldeo.columbia.edu

Award Number : N00014-11-1-0168

Michael L. Banner
School of Mathematics and Statistics, The University of New South Wales, Sydney 2052, Australia
Tel : (+61-2) 9385-7071 fax: (+61-2) 9385-7123 email: m.banner@unsw.edu.au

Russel P. Morison
School of Mathematics and Statistics, The University of New South Wales, Sydney 2052, Australia;
Tel : (+61-2) 9385-7064 fax: (+61-2) 9385-7123 email: r.morison@unsw.edu.au

Award Number: N00014-11-1-0054

LONG-TERM GOALS

We are part of a multi-institutional research team funded by the ONR-sponsored Radiance in a Dynamic Ocean (RaDyO) program. The primary research goals of the program are to (1) examine time-dependent oceanic radiance distribution in relation to dynamic surface boundary layer (SBL) processes; (2) construct a radiance-based SBL model; (3) validate the model with field observations; and (4) investigate the feasibility of inverting the model to yield SBL conditions. Our goals are to contribute innovative measurements, analyses and models of the sea surface roughness at length scales as small as a millimeter. This characterization includes microscale and whitecap breaking waves.

The members of the research team are

Michael Banner, School of Mathematics, UNSW, Sydney, Australia

Johannes Gemmrich, Physics and Astronomy, UVic, Victoria, Canada

Russel Morison, School of Mathematics, UNSW, Sydney, Australia

Howard Schultz, Computer Vision Laboratory, Computer Science Dept, U. Mass., Mass

Christopher Zappa, Lamont Doherty Earth Observatory, Palisades, NY

OBJECTIVES

Nonlinear interfacial roughness elements - sharp crested waves, breaking waves as well as the foam, subsurface bubbles and spray they produce, contribute substantially to the distortion of the optical transmission through the air-sea interface. These common surface roughness features occur on a wide range of length scales, from the dominant sea state down to capillary waves. Wave breaking signatures range from large whitecaps with their residual passive foam, down to the ubiquitous centimeter scale microscale breakers that do not entrain air. There is substantial complexity in the local wind-driven sea surface roughness microstructure, including very steep nonlinear wavelets and breakers. Traditional descriptors of sea surface roughness are scale-integrated statistical properties, such as significant wave height, mean squared slope [e.g., *Cox and Munk*, 1954a] and breaking probability [e.g., *Holthuijsen and Herbers*, 1986]. Subsequently, spectral characterisations of wave height, slope and curvature have been measured, providing a scale resolution into Fourier modes for these geometrical sea roughness parameters. More recently, measurements of whitecap crest length spectral density [e.g., *Gemmrich et al.*, 2008; *Phillips et al.*, 2001] and microscale breaker crest length spectral density [e.g., *Jessup and Phadnis*, 2005] have been reported.

Our effort seeks to provide a more comprehensive description of the physical and optical roughness of the sea surface. We will achieve this through the analysis of our suite of comprehensive sea surface roughness observational measurements within the RADYO field program. These measurements are designed to provide optimal coverage of fundamental optical distortion processes associated with the air-sea interface. In our data analysis, and complementary collaborative effort with RaDyO modelers, we are investigating both spectral and phase-resolved perspectives. These will allow refining the representation of surface wave distortion in present air-sea interfacial optical transmission models.

APPROACH

We build substantially on our accumulated expertise in sea surface processes and air-sea interaction. We are working within the larger team (listed above) measuring and characterizing the surface roughness. This team is contributing the following components to the primary sea surface roughness data gathering effort in RaDyO:

- polarization camera measurements of the sea surface slope topography, down to capillary wave scales, of an approximately 1m x 1m patch of the sea surface (see Figure 1), captured at video rates. [Schultz, Zappa]
- co-located and synchronous orthogonal 75 Hz linear scanning laser altimeter data to provide spatio-temporal properties of the wave height field (resolved to $O(0.5\text{m})$ wavelengths) [Banner, Morison]
- high resolution video imagery to record whitecap data from two cameras, close range and broad field [Gemmrich]
- fast response, infrared imagery to quantify properties of the microscale breakers, and surface layer kinematics and vorticity [Zappa]
- air-sea flux package including sonic anemometer to characterize the near-surface wind speed and wind stress [Zappa]

The team's envisaged data analysis effort includes: detailed analyses of the slope field topography, including mean square slope, skewness and kurtosis; laser altimeter wave height and large scale wave slope data; statistical distributions of whitecap crest length density in different scale bands of propagation speed and similarly for the microscale breakers, as functions of the wind speed/stress and the underlying dominant sea state. Our contributions to the modeling effort will focus on using RaDyO data to refine the sea surface roughness transfer function. This includes the representation of nonlinearity and breaking surface wave effects including bubbles, passive foam, active whitecap cover and spray, as well as micro-breakers.

WORK COMPLETED

Our effort in FY12 comprised further analysis of the suite of atmospheric fluxes and sea surface roughness measurements gathered from FLIP during the RaDyO field experiments in the Santa Barbara channel during September 5-27, 2008 and Hawaii during August 23-September 16, 2009. We participated actively in refining the analysis and validation of the polarimetric and wave breaking data. We also carried out further processing, validation and archiving of our scanning lidar data collocated with our partner investigators' high resolution polarimetric, infrared and optical imaging. This data provides the large scale wave geometry (height and slope) throughout the observational periods.

RESULTS

An overview of results is provided by *Zappa et al.* [2012] and *Dickey et al.* [2012].

TOGA-COARE and Air-sea fluxes

Time series of momentum (wind stress), sensible heat, and water vapor direct covariance fluxes during the Santa Barbara Channel study are shown in the left panel of Figure 1. Also shown are the TOGA-COARE model bulk fluxes [*Fairall et al.*, 2003]. Diurnal processes were the origin of most of the variability in the atmospheric and oceanic forcing. The momentum, sensible heat and latent heat fluxes all show a diurnal cycle similar to the wind speed. Time series of momentum (wind stress), sensible heat, and water vapor direct covariance fluxes during the central Pacific Ocean study south of Hawaii are shown in the right panel of Figure 1. Here, processes were driven by the persistent easterly trade winds.

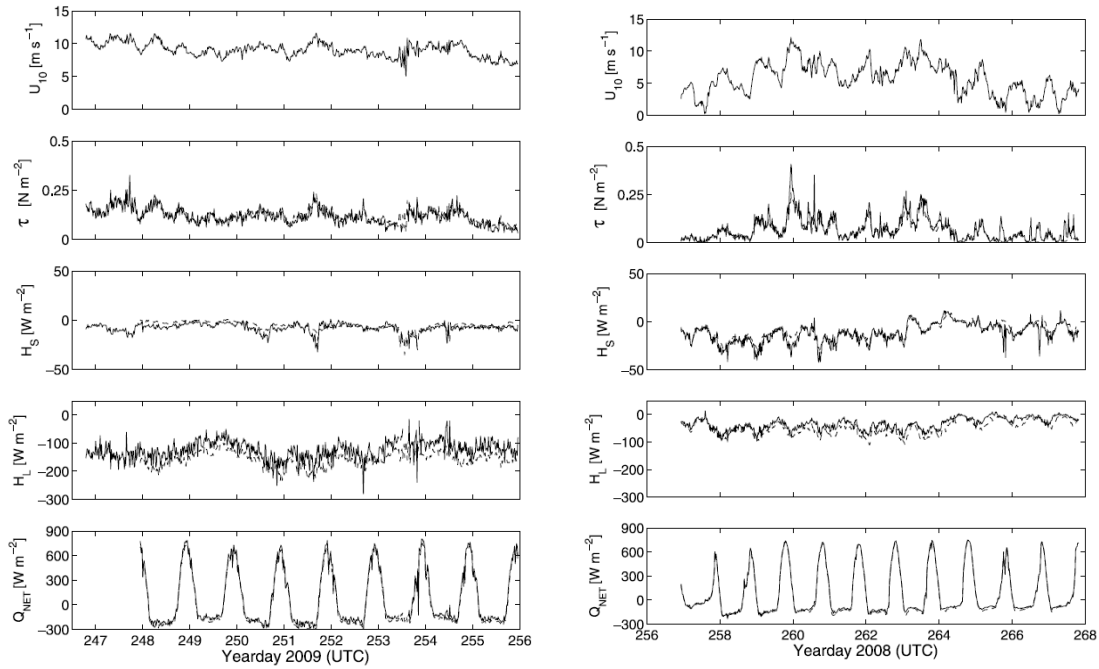


Figure 1. Time series of wind speed U_{10} , momentum flux (wind stress) τ , sensible heat flux H_s , latent heat flux H_l , and net heat flux Q_{net} , during the Santa Barbara Channel experiment (left panel) and during the central Pacific Ocean experiment south of Hawaii (right panel). Solid lines use direct covariance measurements and dashed lines use TOGA-COARE bulk fluxes.

The RaDyO flux data tracks the TOGA-COARE 3.0 model prediction closely. The measured sensible heat flux is within 1.1 W m^{-2} of the TOGA-COARE 3.0 model prediction for SBC and within 2.1 W m^{-2} for the Pacific Ocean south of Hawaii. The TOGA-COARE 3.0 model prediction overestimates the measured latent heat flux by at most 31.6 % for SBC and 21.8 % for the Pacific Ocean south of Hawaii. *Edson* [2008] has observed similar tendencies of this magnitude in his extensive datasets including CLIVar Mode Water Dynamic Experiment (CLIMODE), Coupled Boundary Layer and Air-Sea Transfer (CBLAST) Experiment, Marine Boundary Layer (MBL) Experiment, and Risø Air-Sea Experiment (RASEX). *Edson* is incorporating these observations into the latest TOGA-COARE 4.0 model transfer coefficients where the Dalton number needs to be reduced by up to 25% for winds below 10 m s^{-1} (see Figure 8 in *Edson* [2008]). Thus, the greater overestimation observed in SBC for the latent heat flux is consistent with the larger corrections at lower wind speeds proposed by *Edson* [2008]. Our observations during the RaDyO experiments in SBC and in the Pacific Ocean south of Hawaii provide independent validation of these effects.

We note that the dynamic range of the wind stress is larger during the SBC experiment than the Hawaii experiment. Together these two experiments provide an interesting variety of sea state conditions including light and variable to strongly whitecapping. They provide a valuable test bed for mean square slope and breaking measurements over an interesting dynamic range of wind speeds.

Short ocean wave microstructure

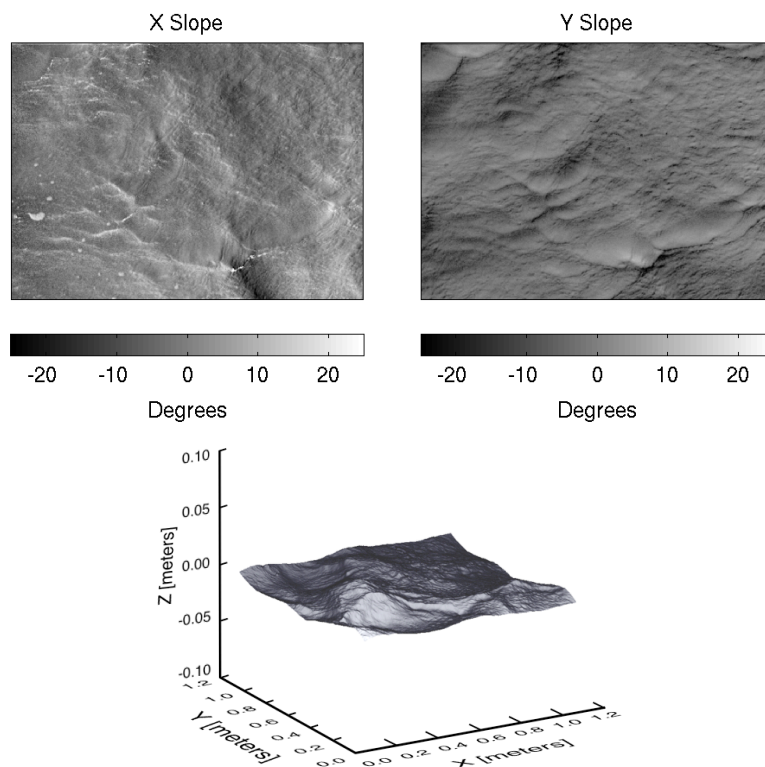


Figure 2. (TOP) A typical gray-scale image of the X- (Left) and Y-Slope (Right) slope field of a small patch of sea surface roughly 1 m by 1m during the Santa Barbara Channel experiment with a wind speed of 9.2 m s^{-1} . (BOTTOM) Representative frame from a video sequence showing a reconstructed wave train for the same data shown in TOP. The spatial resolution is 1.5mm and the temporal resolution is 60Hz.

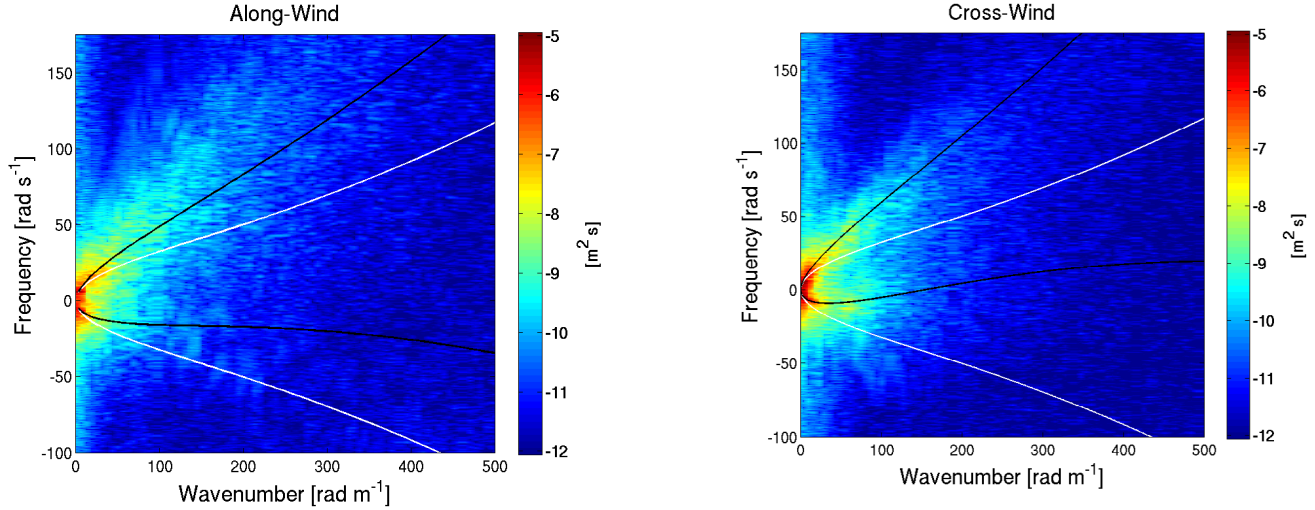


Figure 3. Wavenumber-frequency spectrum from the polarimeter data in the wind (left) and cross-wind (right) directions during the RaDyO Santa Barbara Channel Experiment with a wind speed of 5.5 m s^{-1} and an upper-ocean current speed U_c of 27.3 cm s^{-1} with a relative direction to the wind of 110° . Here, the wind direction and current direction both follow the oceanographic convention of "towards". Positive frequencies are representative of waves propagating in the direction of the forcing. The white trace in each plot is the deep-water dispersion relationship for ocean waves. The black trace in each plot shows that a given wavenumber vector, \vec{k} , is Doppler shifted from its intrinsic frequency, ω_0 , to its observed mean frequency, ω , by $U_c \cdot \vec{k}$, where U_c is the net surface transport velocity for waves of scale \vec{k} . In the absence of along-wind ocean currents, U_c is the wind-drift velocity. U_c is the measured cross-wind ocean current.

Historically, measuring the full two-dimensional, time-varying structure of millimeter scale waves in the open ocean has proven difficult. The major shortcomings of the most remote sensing and in-situ methods have been the inability to extract sufficient information about the full two-dimensional slope field and to construct an instrument that does not disturb the air-sea interface. Figure 2 (TOP) shows sample x- and y-slope images from the Narrow field-of-view Imaging Polarimeter (N-IPol) instrumentation. We captured time-lapsed video at 60 Hz of the X and Y Slope images. A map of the local wave height topography of the imaged patch of the sea surface that is riding on the larger-scale dominant wave is found by integrating the two-dimensional slope field using the method outlined by Frankot and Chellappa [1988] and is shown in Figure 2 (BOTTOM). These slope features are characterized by steep slopes that also have high spatial variance that exhibits a dimpled structure observed previously in the laboratory by Zappa *et al.* [2004]. The N-IPOL has provided useful data on the local directional slope of the gravity waves, and the 1-meter baseline slope intercomparison with the LIDAR slope shows a high (0.8) magnitude squared coherence level. In addition, the polarimeter data characterizes the background environment experienced by the very short wind waves that comprise the sea surface microstructure. These short wave spectra capture data at comparable scales as previously in Hara *et al.* [1998], but without any instrument disturbances to the sea surface. This information allows accurate phasing of the polarimetric camera imagery of the sea surface microstructure with respect to the underlying dominant wind waves. For instance, a new polarimetric

imaging camera highlights the complex interplay of processes in shaping the roughness of the sea surface. These small-scale slope observations by polarimetry highlight the possible oversimplification of the classic Cox-Munk view that mss increases linearly with wind speed (see Figure 3). They suggest the potential importance of upper-ocean currents in addition to the wind. In the wind direction, wave energy follows the deep water dispersion relationship at wave numbers at least up to 100 rad m^{-1} and apparent frequencies up to 40 rad s^{-1} . At higher wave numbers and frequencies the wave energy spreads but does not depart from the mean dispersion curve for zero-mean current. As the wavelength increases, the wind drift influence on propagation decreases, typically vanishing for wavelengths greater than $O(1 \text{ m})$ at moderate wind speeds. The wavenumber-frequency spectrum in the cross-wind direction shows a systematic deviation from the mean dispersion curve for zero-mean current. It is seen that for wave numbers at least up to 100 rad m^{-1} , the slope energy conforms to this Doppler modified dispersion relationship. These results are timely considering issues raised in the recent review article on the conundrums of capillary-gravity waves [Munk, 2009].

Our results are compared with the classical Cox-Munk results [Cox and Munk, 1954a; b] in Figure 4 as well as our more recent laboratory and field measurements using scanning laser slope gauges. We observe the MSS to increase with wind speed, but not linearly as observed by the classic Cox-Munk relationship. We observe more variability than reported by Cox-Munk. Within our measured variability exist noted trends as highlighted by the red, green blue circles (discussed below). Note that the Santa Barbara Experiment results compare well with the Cox-Munk relationships for slick conditions which are consistent with the surfactant levels in the region during the experiment. Publication of the first manuscript demonstrating the feasibility of the polarimetric slope sensing technique was completed. The manuscript was published in Measurement, Science and Technology entitled “Retrieval of short ocean wave slope using polarimetric imaging” [Zappa et al., 2008].

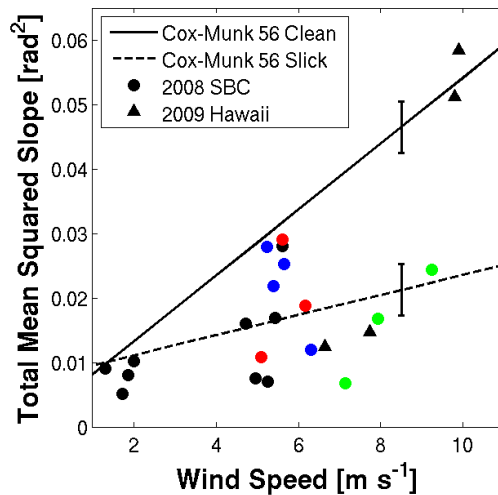


Figure 4. Mean squared total slope against wind speed during the Santa Barbara Channel and Hawaii RaDyO field experiments. The red symbols represent Episode I, the blue symbols represent Episode II, green symbols represent Episode III, and the black symbols represent the rest of the polarimeter data. The solid and dashed lines represent the Cox and Munk [1956] best linear fits to their clean surface and slick-covered surface results. Error bounds on Cox and Munk [1956] best linear fits shown are \pm one standard deviation.

Three Episodes of Local Trends in MSS

The data does not always conform to the linear Cox-Munk relationship of MSS to wind speed, and at times has shown a reversal of the Cox-Munk linear relationship. Furthermore, we observe measurable changes in the directional spectra showing distortion of the short-wave patterns by the currents. This phenomenon has been demonstrated in the wavenumber-frequency spectra examples in Figure 3. In Episode I, the MSS doubles even though the wind speed increases only slightly from 4.6 to 6.5 m⁻¹ and the dominant wind sea does not change. We attribute the increase in mss primarily to the response of the small-scale gravity-capillary waves to the increase in wind speed. Wind speed sensitivity of the spectrum increases toward smaller scales. This underpins the principles of Bragg scatterometry. In Episode II, the MSS halved even though the wind speed increases from 5.2 to 7.1 m s⁻¹. The dominant wind sea decreased and the spectral level is nearly halved over the range of 0.1 to 3.0 Hz. Here, the MSS is less sensitive to smaller scales. In Episode III, the MSS halves and the wind speed decreases from 9.5 to 7.3 m s⁻¹. The dominant wind sea downshifted from 0.25 to 0.20 Hz with an increase of 10% in wave energy. The currents are noted to increase from 6.4 to 20.5 cm s⁻¹ with a direction that is roughly 0° to 20° relative to the wind. The omni-directional wave number slope spectra show the decrease in slope spectral energy was dominated by scales between 7 and 300 rad m⁻¹. Even though a modest increase in the dominant wind sea energy occurs, we attribute the decrease in mss primarily to the response of the small-scale gravity-capillary waves to the decrease in wind speed and the increasing current approximately in the direction of the wind. Co-flowing wind and current tends to reduce the input forcing to the waves, especially for the slower-moving short components, and consequently a reduction in their slope.

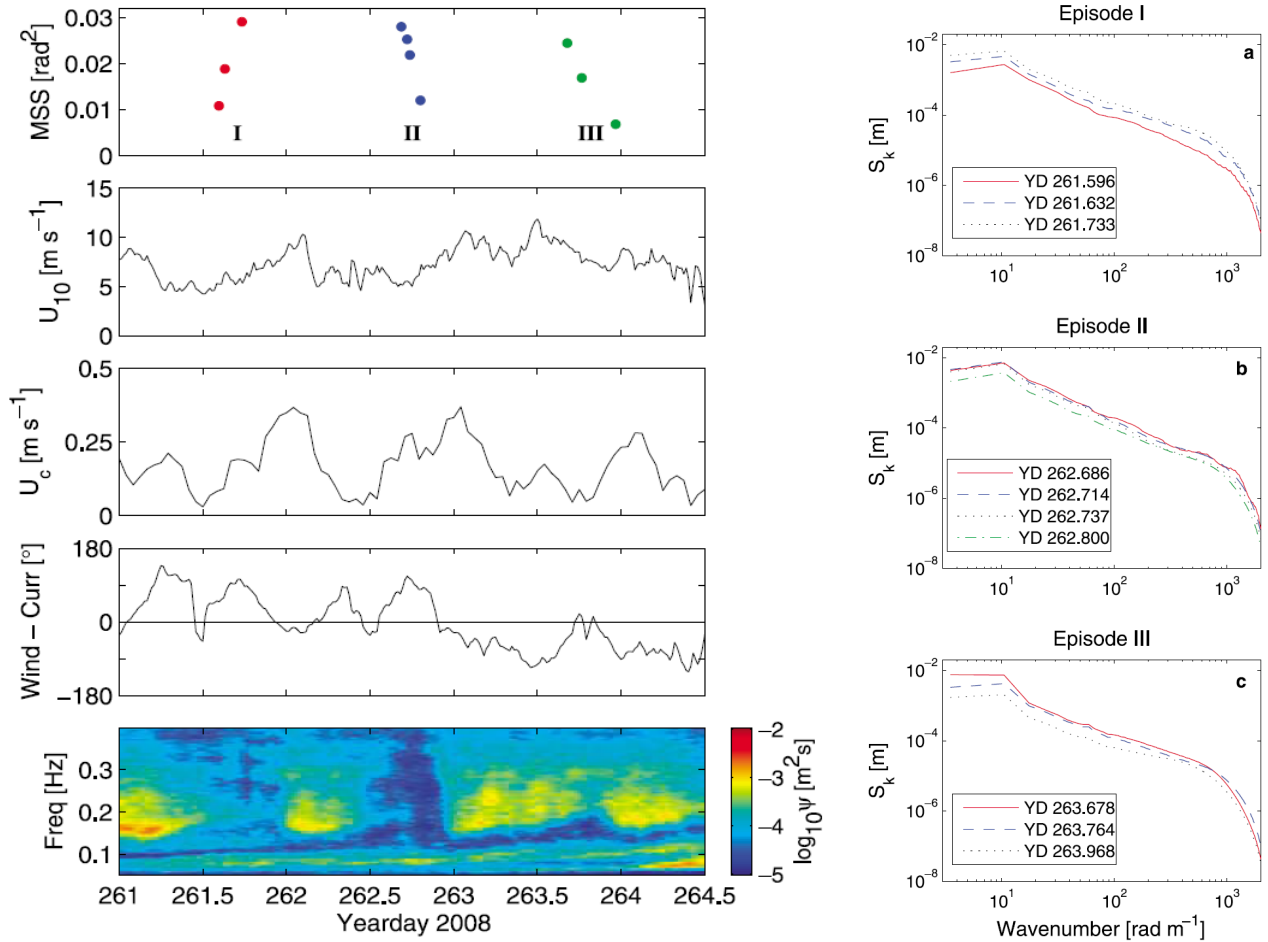


Figure 5. (LEFT) Time series of the total mean square slope (mss), wind speed, ocean current speed, wind direction relative to the current direction, and the wave height spectrogram for a subset of the Santa Barbara Channel experiment. Here the wind direction and current direction both follow the oceanographic convention of “toward.” The color code identifying episodes I, II, and III is the same as in Figure 4. (RIGHT) Omnidirectional wave number spectra for (a) episode I, (b) episode II, and (c) episode III shown on LEFT. The yearday is indicated to highlight the progression of runs within an episode.

Incorporating Surface Roughness Measurements into Modeling

Nonlinear interfacial roughness elements - sharp crested waves, breaking waves as well as the foam, subsurface bubbles and spray they produce, contribute substantially to the distortion of the optical transmission through the air-sea interface. The passage of open ocean whitecaps at different scales shades the subsurface light field transiently. Microbreaking will modulate the refraction of light at the air-sea interface and will contribute minimally to the shading. We have collaborated with **George Kattawar and Yu You** to provide the wave slope data from the N-IPol camera to replace their synthetic wave slope spectra in their simulations [You *et al.*, 2011]. We are also collaborating with **Marlon Lewis** to examine the relevant time-dependent geometrical properties of the surface wave and roughness characteristics as well as the breaking wave front and trailing foam patches including their

spatial and temporal scales. *Wei et al.* [2012] have shown that surface waves have characteristic imprints in irradiance profiles. Specifically, larger waves (with longer wavelengths) are dominant contributors to fluctuations at deeper depths while smaller waves (with shorter wavelengths) are more important in shallower regions in the water column. We examine the effect of wave breaking events on the radiation distribution detected by a subsurface camera (RadCam) at varying depths directly beneath the surface imagery. This effort will provide a far more detailed characterization of the wind driven air-sea interface, including wave breaking (whitecaps and microscale breaking). This is needed to provide more complete parameterizations of these processes, which will improve the accuracy of ocean optical radiative transfer models and trans-interfacial image reconstruction techniques.

IMPACT/APPLICATIONS

This effort will provide a far more detailed characterization of the wind driven air-sea interface, including wave breaking (whitecaps and microscale breaking). This is needed to provide more complete parameterizations of these processes, which will improve the accuracy of ocean optical radiative transfer models and trans-interfacial image reconstruction techniques.

REFERENCES

- Cox, C., and W. Munk (1954a), Measurement of the roughness of the sea surface from photographs of the sun's glitter, *Journal of the Optical Society of America*, 44(11), 838-850.
- Cox, C., and W. Munk (1954b), Statistics of the sea surface derived from sun glitter, *Journal of Marine Research*, 13(2), 198-227.
- Cox, C., and W. Munk (1956), Slopes of the sea surface deduced from photographs of sun glitter, *Bulletin of the Scripps Institution of Oceanography*, 6(9), 401-487.
- Dickey, T., et al. (2012), Introduction to special section on Recent advances in the study of optical variability in the near-surface and upper ocean, *Journal of Geophysical Research – Oceans*, 117(C00H20), doi:10.1029/2012JC007964.
- Edson, J. B. (2008), Review of Air-Sea Transfer Processes, in *ECMWF Workshop on Ocean-Atmosphere Interactions*, edited, pp. 7-25, European Centre for Medium Range Forecasts, Reading, UK.
- Fairall, C. W., E. F. Bradley, J. E. Hare, A. A. Grachev, and J. B. Edson (2003), Bulk parameterization of air-sea fluxes: Updates and verification for the COARE algorithm, *J. Climate*, 16, 571-591.
- Gemmrich, J. R., M. L. Banner, and C. Garrett (2008), Spectrally resolved energy dissipation and momentum flux of breaking waves, *J. Phys. Oceanogr.*, 38, 1296-1312.
- Hara, T., E. J. Bock, J. B. Edson, and W. R. McGillis (1998), Observation of short wind waves in coastal waters, *Journal of Physical Oceanography*, 28(7), 1425-1438.
- Holthuijsen, L. H., and T. H. C. Herbers (1986), Statistics of breaking waves observed as whitecaps in the open sea, *Journal of Physical Oceanography*, 16, 290-297.
- Jessup, A. T., and K. R. Phadnis (2005), Measurement of the geometric and kinematic properties of microscale breaking waves from infrared imagery using a PIV algorithm, *Meas. Sci. Technol.*, 16, 1961-1969.

- Munk, W. (2009), An inconvenient sea truth: Spread, steepness, and skewness of surface slopes, *Annu. Rev. Mar. Sci.*, 1 (doi: 10.1146/annurev.marine.010908.163940), 377–415.
- Phillips, O. M., F. L. Posner, and J. P. Hanson (2001), High resolution radar measurements of the speed distribution of breaking events in wind-generated ocean waves: surface impulse and wave energy dissipation rates, *J. Phys. Oceanogr.*, 31, 450–460.
- Wei, J., M. Lewis, R. V. Dommelen, C. J. Zappa, and M. Twardowski (2012), Signatures of wave-induced light field fluctuations in measured irradiance depth profiles, *Journal of Geophys. Res.*, submitted.
- You, Y., G. W. Kattawar, K. J. Voss, P. Bhandari, J. Wei, M. Lewis, C. J. Zappa, and H. Schultz (2011), Polarized light field under dynamic ocean surfaces: Numerical modeling compared with measurements, *Journal of Geophysical Research – Oceans*, 116(C00H05), doi:10.1029/2011JC007278.
- Zappa, C. J., W. E. Asher, A. T. Jessup, J. Klinke, and S. R. Long (2004), Microbreaking and the enhancement of air-water transfer velocity, *J. Geophys. Res.*, 109(C08S16), doi:10.1029/2003JC001897.
- Zappa, C. J., M. L. Banner, H. Schultz, A. Corrada-Emmanuel, L. B. Wolff, and J. Yalcin (2008), Retrieval of short ocean wave slope using polarimetric imaging, *Measurement Science and Technology*, 19(055503), doi:10.1088/0957-0233/1019/1085/055503.
- Zappa, C. J., J. R. Gemmrich, R. P. Morison, H. Schultz, M. L. Banner, D. A. LeBel, and T. Dickey (2012), An overview of sea state conditions and air-sea fluxes during RaDyO, *Journal of Geophysical Research – Oceans*, 117, doi:10.1029/2011JC007336.

PUBLICATIONS

- Dickey, T., et al. (2012), Introduction to special section on Recent advances in the study of optical variability in the near-surface and upper ocean, *Journal of Geophysical Research – Oceans*, 117(C00H20), doi:10.1029/2012JC007964. [published, refereed].
- Wei, J., M. Lewis, R. V. Dommelen, C. J. Zappa, and M. Twardowski (2012), Signatures of wave-induced light field fluctuations in measured irradiance depth profiles, *Journal of Geophys. Res.*, [submitted, refereed].
- You, Y., G. W. Kattawar, K. J. Voss, P. Bhandari, J. Wei, M. Lewis, C. J. Zappa, and H. Schultz (2011), Polarized light field under dynamic ocean surfaces: Numerical modeling compared with measurements, *Journal of Geophysical Research – Oceans*, 116(C00H05), doi:10.1029/2011JC007278. [published, refereed].
- Zappa, C. J., M. L. Banner, H. Schultz, A. Corrada-Emmanuel, L. B. Wolff, and J. Yalcin (2008), Retrieval of short ocean wave slope using polarimetric imaging, *Measurement Science and Technology*, 19(055503), doi:10.1088/0957-0233/1019/1085/055503. [published, refereed].
- Zappa, C. J., J. R. Gemmrich, R. P. Morison, H. Schultz, M. L. Banner, D. A. LeBel, and T. Dickey (2012), An overview of sea state conditions and air-sea fluxes during RaDyO, *Journal of Geophysical Research – Oceans*, 117, doi:10.1029/2011JC007336. [published, refereed].